Cytometry
PART A
Journal of the International Society for Advancement of Cytometry

A Novel Quantitative Volumetric Spreading Index Definition and Assessment of Astrocyte Spreading In Vitro

Volkan Müjdat Tiryaki,[1]* Virginia M. Ayres,[2] Ijaz Ahmed,[3] David I. Shreiber[3]

[1]Department of Computer Engineering, School of Engineering and Architecture, Siirt University, Siirt 56100, Turkey

[2]Department of Electrical and Computer Engineering, Michigan State University, East Lansing, Michigan 48824

[3]Department of Biomedical Engineering, Rutgers, The State University of New Jersey, Piscataway, New Jersey 08854

Grant sponsor: National Science Foundation (VMA and VMT), Grant number: PHY-0957776

Grant sponsor: National Science Foundation (DIS and IA), Grant number: ARRA-CBET-0846328

Additional Supporting Information may be found in the online version of this article.

*Correspondence to: Volkan Müjdat Tiryaki, School of Engineering and Architecture, Block B, Siirt University Kezer Campus, Siirt 56100, Turkey. Email: tiryakiv@siirt.edu.tr

Published online 00 Month 2017 in Wiley Online Library (wileyonlinelibrary.com)

DOI: 10.1002/cyto.a.23183

Abstract

A novel quantitative volumetric spreading index (*VSI*) is defined that depends on the total distance between object voxels and the contact surface plane in three-dimensional (3D) space. The *VSI*, which ranges from 0 to 1, is rotationally invariant around the *z*-axis. *VSI* can be used to quantify the degree of individual cell spreading, which is important for analysis of cell interactions with their environment. The *VSI*s of astrocytes cultured on a nanofibrillar surface and three different comparative planar surfaces have been calculated from confocal laser scanning microscope z-series images, and the effects of both culture surface and immunoreactivity on the degree of cell spreading were investigated. *VSI* calculations indicated a statistical correlation between increased reactivity, based on immunolabeling for glial fibrillary acidic protein, and decreased cell spreading. Further results provided a quantitative measure for the increased spreading of quiescent-like and reactive-like astrocytes on planar substrates functionalized with poly-L-lysine. © 2017 International Society for Advancement of Cytometry

Key terms

cell morphology; quantitative cell spreading; 3D shape descriptor; immunoreactivity; confocal laser scanning microscope

Introduction

Cell cultures are used for studying cell behaviors in controlled environments. Cell spreading, also known as cell flattening, is a result of cell and surface interactions initiated by cell adhesion. The degree of cell spreading is an important component of cell interactions with the environment; however, only a few methods to rigorously quantify individual cell spreading are available. In some cell spreading studies, cells were categorized by human observation as belonging to two to four classes depending on the degree of spreading, and the percentage in each class was determined to calculate a cell spreading index (1–3). In other studies, cell spreading area (4–6) and cell perimeter measurements (7) were used to quantify the cell spreading. Although these methods are practical and easy to implement, the quantitative degree of single cell volumetric spreading is partly ignored. Farooque et al. (8) proposed a dimensionality matrix to assess gyration tensor ellipsoids that are fit to each cell, and then classified the ellipsoids as 1D, 2D, or 3D. This measure can be used to quantitatively estimate the cell spreading behavior for cell types that are dominated by the cell soma response. However, for process-bearing cells such as neurons and astrocytes, the cell process extension response beyond the cell soma is also important. A cell shape index recently proposed by Tiryaki et al. quantifies both stellation and spreading together but is sensitive to cell surface area changes (9).

In the present work, a new volumetric spreading index (*VSI*) is defined that depends on the total distances between object voxels and the contact surface plane.

ISAC
International Society for Advancement of Cytometry

The new *VSI* does not directly depend on the object surface area, is rotationally invariant around the *z*-axis and has a range between 0 and 1 with clear and intuitive interpretation.

In this investigation, the new *VSI* is first introduced and investigated for sensitivity to changes in discretization and changes in scale. It is then used to quantify the degree of spreading by astrocytes on substrates with different properties that were previously shown to influence spreading (10).

Materials and Methods

Nanofibrillar Scaffolds and Comparative Culture Surfaces

Poly-L-lysine-functionalized planar glass (PLL glass), unfunctionalized planar Aclar (Aclar), PLL-functionalized planar Aclar (PLL Aclar), and polyamide nanofibrillar scaffolds were prepared (9). Glass (12 mm, No. 1 coverglass; Fisher Scientific, Pittsburgh, PA) or Aclar coverslips (12 mm; Ted Pella, Redding, CA) were placed in a 24-well tissue culture plate (one coverslip/well) and covered with 1 ml of PLL solution (50 μg PLL/mL in dH_2O) overnight. The coverslips used for the cultures were then rinsed with dH_2O and sterilized with 254 nm UV light using a Spectronics Spectrolinker XL-1500 (Spectroline Corporation, Westbury, NY). The polyamide nanofibrillar scaffolds electrospun on Aclar substrates were obtained from Donaldson (Minneapolis, MN) and Corning Life Sciences (Lowell, MA). The nanofiber diameter range of nanofibrillar scaffolds is from ∼100 to ∼300 nm. Promising in vivo and in vitro results have been obtained for astrocytes in contact with these nanofibrillar scaffolds, as implants or as culture surfaces (10–12).

Primary Quiescent-like and Reactive-like Astrocyte Cultures

Primary quiescent-like astrocyte cultures were prepared from new born Sprague Dawley (postnatal day 1 or 2) rats (9,10). All procedures were approved by the Rutgers Animal Care and Facilities Committee (IACUC Protocol #02–004). The rat pups were sacrificed by decapitation, and the cerebral hemispheres were isolated aseptically. The cerebral cortices were dissected out, freed of meninges, and collected in Hank's buffered saline solution (HBSS; Mediatech, Herndon, VA). The cerebral cortices were then minced with sterile scissors and digested in 0.1% trypsin and 0.02% DNase for 20 min at 37°C. The softened tissue clumps were then triturated by passing several times through a fine bore glass pipette to obtain a cell suspension. The cell suspension was washed twice with culture medium (Dulbecco's Modified Eagle's Medium [DMEM]; Life Technologies, Carlsbad, CA + 10% fetal bovine serum [FBS]; Life Technologies) and filtered through a 40-μm nylon mesh. For culturing, the cell suspension was placed in 75 cm^2 flasks (one brain/flask in 10 mL growth medium) and incubated at 37°C in a humidified CO_2 incubator. After 3 days of incubation, the growth media were removed, cell debris was washed off, and fresh medium was added. The medium was changed every 3–4 days. After reaching confluency (7 days), the cultures were shaken to remove macrophages and other loosely adherent cells.

To obtain reactive-like astrocytes, 0.25 mM dibutyryl cyclic adenosine monophosphate (dBcAMP) was added to the culture medium of 7-day-old semiconfluent quiescent astrocyte cultures and the serum concentration was reduced to 1%. The cultures in dBcAMP containing medium were incubated for additional 7–8 days with a media change every 3–4 days. The morphology of the cells was observed on alternate days under a phase contrast microscope. In the control cultures, the cells were fed with DMEM + 1% FBS (without dBcAMP).

Quiescent-like and reactive-like astrocytes were harvested at the same time point using 0.25% trypsin/ethylene-diaminetetraacetic acid (EDTA; Sigma-Aldrich, St. Louis, MO) and reseeded at a density of 30,000 cells/well directly on 12-mm Aclar or PLL Aclar coverslips, PLL glass coverslips, or on Aclar coverslips coated with nanofibers in 24-well plates in astrocyte medium containing dBcAMP (0.5 ml). After culturing the astrocytes on the aforementioned substrates for 24 h, they were fixed with 4% paraformaldehyde for 10 min. Parallel cultures were immunostained with glial fibrillary acidic protein (GFAP), an identification marker for astrocytes, and >95% were found to be GFAP-positive.

Confocal Laser Scanning Microscope Imaging

Confocal z-series images were captured using an Olympus FluoView 1000 CLSM system attached to an Olympus IX81 automated inverted microscope platform equipped with a 40× oil immersion objective (NA = 1.3). The z-series were acquired under identical imaging conditions, including the same high voltage, offset and gain settings, same objective, and same resolution (1024 × 1024 pixels). The intensity data were collected from samples in three dimensions. The z-step size was set to 1.13 μm as described in Ref. (11). Fifty cells were analyzed for each culture surface and immunoreactivity situation, making a total of 400 astrocytes. GFAP immunostained images were used for the quantitative cell spreading analysis.

Quantitative Astrocyte Spreading Assessment by *VSI*

A face-connected voxel model was created for each cell in the CLSM data. The CLSM imaging conditions were carefully set so that the background pixel illumination was almost zero. The raw CLSM GFAP data was segmented using simple thresholding ($T > 0$). After segmentation of each z-slice, thresholding was used to isolate individual cells and cell clusters, with further segmentation of cells in clusters performed by hand. The volumetric data for each cell was obtained using the assembly of z-series slices and was represented by the means of a spatial occupancy array, defined in Bribiesca (13). The unit voxel dimensions for images taken with a 40× objective was 0.3097 μm × 0.3097 μm × 1.13 μm in *x*–*y*–*z*. Since there is approximately fourfold difference between the axial and lateral resolution, the 3D data were upsampled to obtain nearly cubic unit voxels using cubic interpolation. Implementation was done using the "interp3" command of MATLAB.

Results

VSI

The new *VSI* is defined as the exponential of negative total voxel distance to the contact surface plane where the total distance is normalized according to a cube:

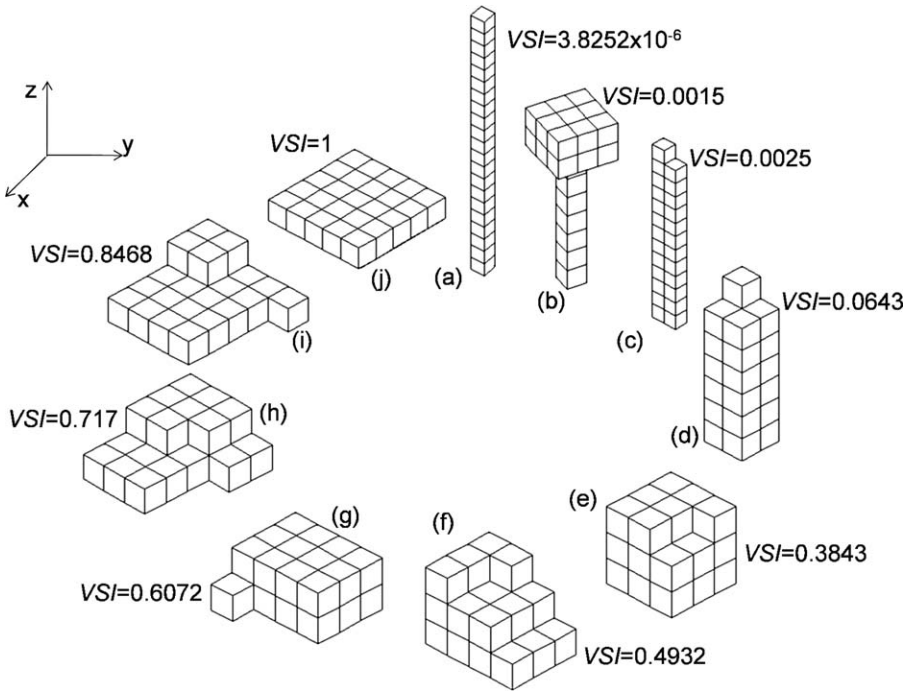

Figure 1. *VSI* measurements for objects having a total of $N = 25$ voxels represented by unit cubes. (**a**) *VSI* is close to 0 for the 1D object which is normal to the $z = 0$ plane. (**b–i**) *VSI* increases gradually in clock-wise direction as "spreading" increases. (**j**) *VSI* is 1 when the object is completely spread.

$$VSI = \begin{cases} e^{-\frac{2\sum_{v\in V_c}\left(z/u\right)}{N\left(\sqrt[3]{N}-1\right)}} & \text{if } N \neq 1 \\ 1 & \text{if } N = 1 \end{cases} \quad (1)$$

where v is an object voxel, V_c is the set of all object voxels, N is the total number of object voxels, z is the minimum distance between voxel v and the contact surface plane, and u is the unit voxel length. An object is considered as a series of z-slices that are parallel to the *xy*-plane. The exponential formulation ensures that *VSI* is between 0 and 1. The normalization factor $N\left(\sqrt[3]{N}-1\right)/2$ is the total voxel distances of a cube with edge length $\sqrt[3]{N}$ unit voxels to the contact surface plane. A cube has equal edge lengths, and therefore, the *VSI* should be constant and equal to e^{-1} for any cube.

VSI ranges from 0 to 1 and has an inverse correlation with the total distance between object voxels and the contact surface plane. The MATLAB codes for a tutorial example *VSI* calculation are given in Section 1 of Supporting Information (14).

VSI calculations for a set of 10 test objects each having 25 voxels in different "spreading" arrangements are shown in Figure 1. The *VSI* is, correctly, equal to 1 when all voxels are in a single plane. The *VSI* increases as the "spreading" increases, and it is close to 0 for the 1D voxel configuration normal to the *xy*-plane.

Investigation of a set of semiellipsoid objects having more cell-realistic numbers and voxel arrangements is shown in Figure 2. The *VSI* gradually increases as the "spreading" increases when the "volume" is held almost constant in approximation of real spreading behavior (15).

The sensitivities of the new *VSI* to discretization and to size were also investigated. For the discretization investigation, cubes and spheres with, respectively, 64 unit voxel side lengths or diameters were analyzed. *VSI*s were measured as a function of decreasing unit voxel length. The results in Figure 3a show that the new *VSI* is ideally insensitive to discretization when the object of interest is a cube and only slightly sensitive (<0.3%) to discretization when the object of interest is a sphere.

For the size investigation, *VSI*s of cubes and spheres were measured as a function of increasing side or diameter length from 4 up to 64 voxels. The results in Figure 3b show that the *VSI* is ideally scale-invariant when the object of interest is a cube, and only slightly sensitive (<0.1%) to scale when the object of interest is a sphere.

VSI measurements are intuitive because *VSI* of a cube is higher than the *VSI* of a sphere having a comparable dimension with the cube. The codes for sensitivity investigation of *VSI* are given in Section 1.2 of Supporting Information.

Astrocyte Morphology Investigation by *VSI*

The *VSI* definition given in Equation (1) was used for a comparative investigation of the quantitative spreading of cerebral cortical astrocytes cultured on the four different culture surfaces that presented different nano-physical cues (10,11). These were PLL glass, Aclar, PLL Aclar, and polyamide nanofibrillar scaffolds.

The *VSI*s of astrocytes cultured on the three planar surfaces and the nanofibrillar surface were calculated from CLSM

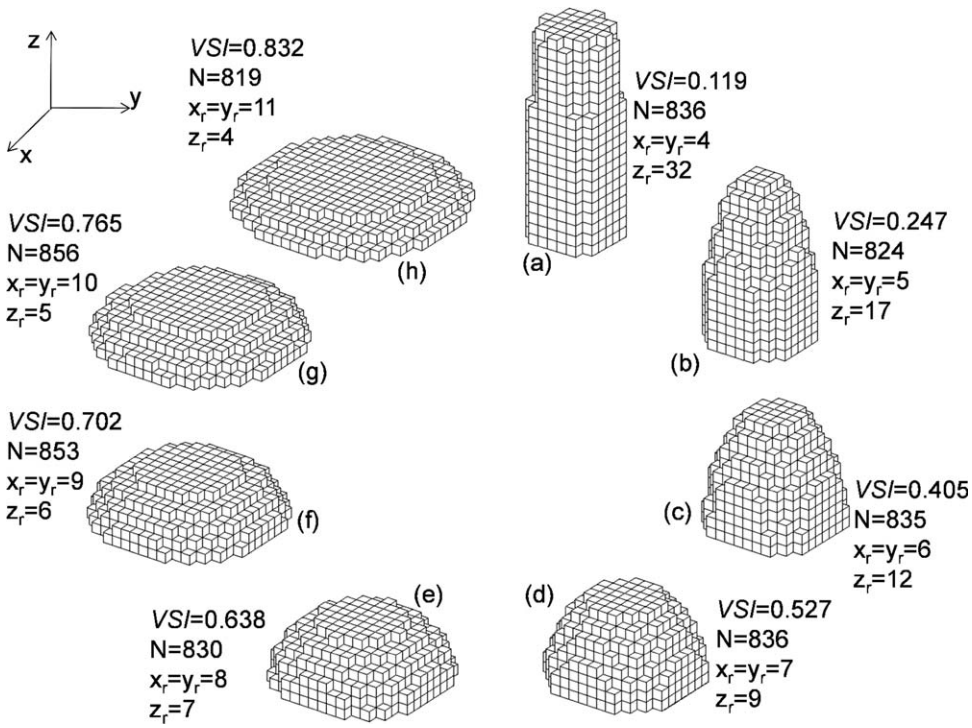

Figure 2. Quantitative spreading of eight filled semiellipsoids determined using *VSI*. The ellipsoids' semiaxes in *xy* direction are gradually increasing and semiaxes in *z* dimension are simultaneously decreasing so that the volume is almost constant from (**a**) to (**h**) in the clockwise direction. Semiaxes lengths, x_r, y_r, and z_r, are given in voxels, and *N* is the total number of voxels. Center of each ellipsoid is at (0,0,0).

z-series images. Comparison of the *VSI*s enabled quantitative investigation of the effects of the environments and also the effects of dBcAMP-treatment on the degree of cell spreading. Variations in the *VSI* data among the culture surfaces were analyzed using two-way ANOVA followed by pairwise post hoc comparisons with Tukey's test and all statistically significant differences were identified. Significance levels were set at $P < 0.05$. Results show that both immunoreactivity level and material type have significant effects on *VSI*. Material type and reactivity level interaction has a significant effect on *VSI*. The details of the two-way ANOVA can be found in Section 2 of Supporting Information.

The bar plots given in Figure 4 showed that the *VSI*s of quiescent- and reactive-like astrocytes on PLL Aclar were significantly higher than all other surfaces. Figure 4 results also indicated that the dBcAMP treatment significantly reduced the *VSI*s of astrocytes cultured on Aclar and nanofibrillar scaffolds. The increased astrocyte reactivity was correlated to a decrease in cell spreading in vitro.

The lowest *VSI* was observed for reactive-like astrocytes on the Aclar substrate. It indicates a weak cell-substrate interaction, which is consistent with our previous results (9). A representative 3D plot rendered in unit cube voxels of an astrocyte cultured on Aclar with a *VSI* of 0.711 is shown in Figure 5.

Comparison of New *VSI* with *CSI-V*

A volumetric cell shape index (*CSI-V*) was previously defined by our group (9) as

$$CSI-V = \frac{SA_{cell}^3}{60.75\pi V_{cell}^2} \quad (2)$$

where SA_{cell} is the cell surface area and V_{cell} is the cell volume. When its performance was compared to a conventional two-dimensional CSI (16), it was shown that inclusion of the volumetric information about the cell spreading behavior led to different and more accurate biomedical conclusions. *CSI-V* quantifies both cell spreading and stellation together, but it is not able to separate the spreading and stellation response of a cell, whereas the *VSI* is a specific shape descriptor that quantifies individual cell spreading. *CSI-V* depends on the object surface area, whereas *VSI* formula does not depend on the object surface area. In conclusion, *VSI* is better than *CSI-V* for cell spreading quantification. Comparison of *VSI* of the present study and *CSI-V* based on sensitivity, origin, range, and other criteria is shown in Table 1. Comparisons of *CSI-V*s and *VSI*s of representative astrocytes together with binary projection images on *xy*-, *xz*-, and *yz*-planes are given in Section 3 of Supporting Information.

Discussion

There is a need for a 3D volumetric cell shape descriptor that provides an accurate and quantitative determination of the degree of cell spreading. Cell spreading analysis in 3D is important and has been hindered by the lack of a metric. The new *VSI* in Equation (1) is straightforward to calculate with a clear and intuitive interpretation. It can be used for 3D cell shape analysis and more generally for 3D object classification.

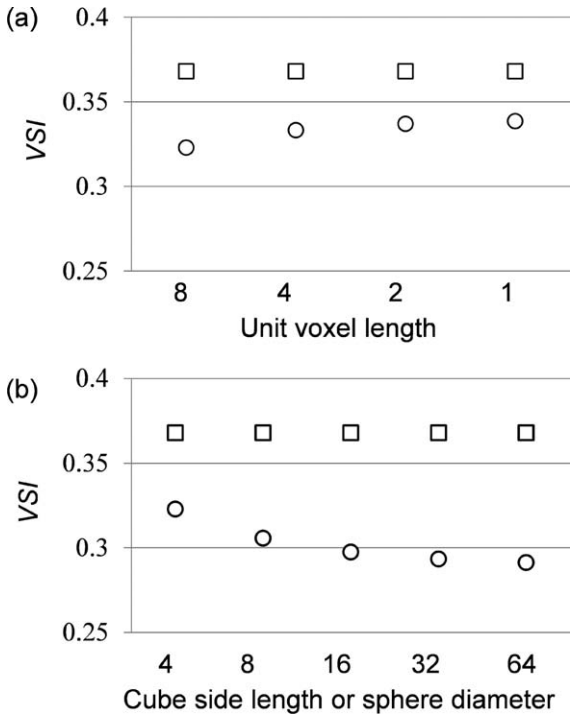

Figure 3. Sensitivity of *VSI* on discretization (**a**) and object size (**b**). (a) *VSI* of cubes and spheres which have 64 unit voxels side length or diameter. *VSI* is insensitive to discretization when the object is a cube (constant and equal to e^{-1}), and slightly sensitive to discretization when the object is a sphere. (b) *VSI* of a cube is insensitive to object size (constant and equal to e^{-1}), and *VSI* of a sphere is slightly sensitive to object size. Unit voxel length is constant and equal to one unit. Square and circle points on both graphs show measurements from sphere and cube, respectively.

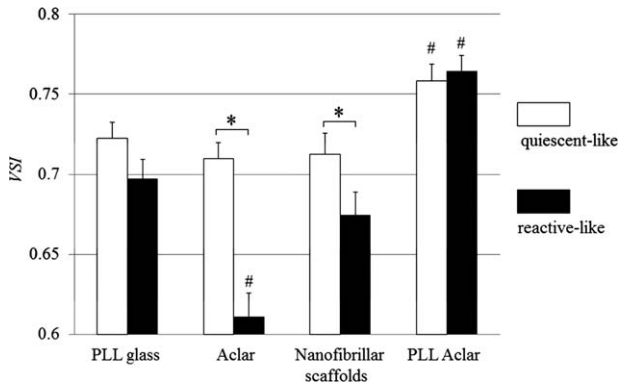

Figure 4. Mean *VSI* results for quiescent-like and reactive-like astrocytes. Error bars show standard error of the mean of $n = 50$ astrocytes. * denotes significance, $P < 0.05$; # denotes significance from all other culture surfaces for the same type of immunoreactivity group, $P < 0.05$.

In this study, the new *VSI* performance was first investigated using two sets of synthetic objects and it produced logically consistent results. The new *VSI* was shown to be minimally sensitive to discretization and size. Although cubes and spheres were used here as test objects, they demonstrate the potential that the new *VSI* has to contribute quantitative understanding in real cell investigations including cubic and columnar epithelial cell growth in organ repair/regeneration (17), improved bone marrow cell production from cubic scaffold environments (18), assumption of pathological cube-like morphologies by renal cancer cells (19), and assumption of nonadherent and drug-resistant sphere-like morphologies by various tumor-initiating cells (20).

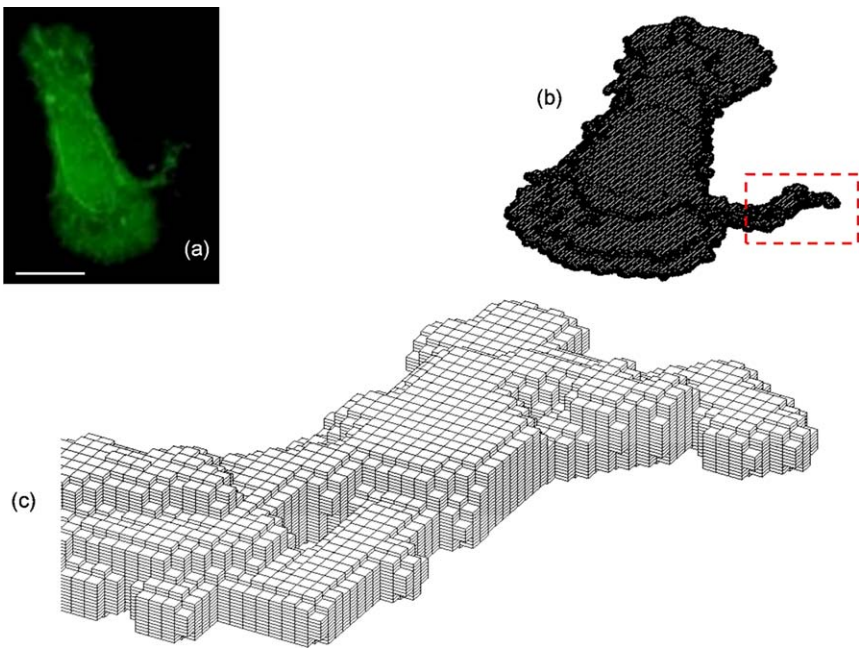

Figure 5. (**a**) Maximum-intensity projection GFAP staining image of a quiescent-like astrocyte cultured on Aclar. Scale bar, 10 μm. (**b**) 3D plot of the astrocyte composed of 406,960 unit cube voxels. The *VSI* of the cell is 0.711. (**c**) A close-up image of the astrocyte process shown by dashed-box in (b). [Color figure can be viewed at wileyonlinelibrary.com]

Table 1. Comparison of *CSI-V* and *VSI* based on different criteria

CRITERION	CSI-V	VSI
Quantification	Spreading and stellation	Spreading
Origin	Classical compactness measure	Exponential of negative total voxel distance to the contact surface plane normalized according to a cube
Range	1 to $+\infty$	0–1
Rotationally invariance	Yes	Rotationally invariant around *z*-axis
Translational invariance	Yes	Yes for objects on the $z = 0$ plane
Invariance to discretization	No	Yes for a cube, only minimal difference for a sphere
Scale invariance	No	Yes for a cube, only minimal difference for a sphere
Sensitivity to surface area	Yes	Does not directly depend on object surface area

The new *VSI* was then used to quantitatively characterize the spreading of astrocytes in different culture environments and in different immunoreactivity states. The *VSI* results in Figure 4 and the quantitative GFAP immunoreactivity analysis of our recent study (11) show that there is a negative correlation between the *VSI* and immunoreactivity of astrocytes. That reduced *VSI* appears to be correlated with increase in the dBcAMP-induced immunoreactivity indicates that the cAMP dependent signaling pathway may influence the astrocyte-environment (substrate or scaffold) interactions and the astrocyte cytoskeleton.

Confocal and super-resolution microscopies, which are relatively new in the biomedical community, provide high-resolution volumetric data which is suitable for quantitative and accurate assessment of individual cell spreading. The axial resolution of CLSM is currently lower than the lateral resolution; the approximately fourfold difference between the axial and lateral resolution in the present study was addressed by up-sampling in the *z*-direction using cubic interpolation to obtain nearly cubic unit voxels. New developments in super resolution microscopy have substantially improved the asymmetry situation through improvements in the axial resolution as well as in the lateral resolution. Stimulated emission depletion microscopy combined with 4Pi microscopy (two opposing objectives for excitation and detection) can achieve axial resolutions of 30–40 nm, with lateral resolutions of ∼30 nm. Stochastic optical reconstruction microscopy, photoactivated localization microscopy, and fluorescence photoactivation localization microscopy can achieve axial resolutions of ∼50 nm with lateral resolutions of ∼20 nm. In addition to higher resolving power, axial and lateral resolutions are becoming more symmetric (21). The new *VSI* is ideal for cell spreading analysis of images acquired using super resolution microscopy, and we will report investigations in a future study.

Conflicts of Interest

The authors declare that there are no conflicts of interest.

Literature Cited

1. Chen P, McGuire K, Hackman RC, Kim KH, Black RA, Poindexter K, Yan W, Liu P, Chen AJ, Parks WC, et al. Tissue inhibitor of metalloproteinase-1 moderates airway re-epithelialization by regulating matrilysin activity. Am J Pathol 2008;172:1256–1270.
2. Wang C, Dawes LJ, Liu Y, Wen L, Lovicu FJ, McAvoy JW. Dexamethasone influences FGF-induced responses in lens epithelial explants and promotes the posterior capsule coverage that is a feature of glucocortacoid-induced cataract. Exp Eye Res 2013; 111:79–87.
3. Angel del Pozo M, Schwartz MA, Hu J, Kiosses WB, Altman A, Villalba M. Guanine exchange-dependent and -independent effects of Vav1 on integrin-induced T cell spreading. J Immunol 2003;170:41–47.
4. Vishavkarma R, Raghavan S, Kuyyamudi C, Majumder A, Dhawan J, Pullarkat PA. Role of actin filaments in correlating nuclear shape and cell spreading. PLoS One 2014;9:e107895.
5. Lehnert D, Wehrle-Haller B, David C, Weiland U, Ballestrem C, Imhof BA, Bastmeyer M. Cell behaviour on micropatterned substrata: limits of extracellular matrix geometry for spreading and adhesion. J Cell Sci 2004;117:41–52.
6. Tumova M, Koffer A, Simicek M, Draberova L, Draber P. The transmembrane adaptor protein NTAL signals to mast cell cytoskeleton via the small GTPase Rho. Eur J Immunol 2010;40:3235–3245.
7. Brugmans M, Cassiman JJ, Vanderheydt L, Oosterlinck AJJ, Vlietinck R, Berghe HVD. Quantification of the degree of cell spreading of human fibroblasts bv semi-automated analysis of the cell perimeter. Cytometry 1982;3:262–268.
8. Farooque TM, Camp CH, Tison CK, Kumar G, Parekh SH, Simon CG. Measuring stem cell dimensionality in tissue scaffolds. Biomaterials 2014;35:2558–2567.
9. Tiryaki VM, Adia-Nimuwa U, Ayres VM, Ahmed I, Shreiber DI. Texture-based segmentation and a new cell shape index for quantitative analysis of cell spreading in AFM images. Cytometry Part A 2015;87A:1090–1100.
10. Tiryaki VM, Ayres VM, Khan AA, Ahmed I, Shreiber DI, Meiners S. Nanofibrillar scaffolds induce preferential activation of Rho GTPases in cerebral cortical astrocytes. Int J Nanomed 2012;7:3891–3905.
11. Tiryaki VM, Ayres VM, Ahmed I, Shreiber DI. Differentiation of reactive-like astrocytes cultured on nanofibrillar and comparative culture surfaces. Nanomedicine 2015;10:529–545.
12. Meiners S, Harris SL, Delgado-Rivera R, Ahmed I, Babu AN, Patel RP, Crockett DP. A nanofibrillar prosthetic modified with fibroblast growth factor-2 for spinal cord repair. In: Chang WN, editor. Nanofibers: Fabrication, Performance, and Applications. Hauppage, NY: Nova Science Publishers; 2009. pp 327–343.
13. Bribiesca E. A measure of compactness for 3D shapes, computers and mathematics with applications. Comput Math Appl 2000;40:1275–1284.
14. MathWorks Support Team. 3D plot of solid object built from tiny cubes. Available at http://www.mathworks.com/matlabcentral/newsreader/view_thread/236226. Accessed on 03.05.2016.
15. Lodish H, Berk A, Kaiser CA, Krieger M, Scott MP, Bretscher A, Ploegh H, Matsudaira P. Molecular Cell Biology, 6th ed. New York, NY: W H Freeman and Company; 2008, Chapter 17.
16. Matsutani S, Yamamoto N. Neuronal regulation of astrocyte morphology in vitro is mediated by GABAergic signaling. Glia 1997;20:1–9.
17. Vrana NE, Lavalle P, Dokmeci MR, Dehghani F, Ghaemmaghami AM, Khademhosseini A. Engineering functional epithelium for regenerative medicine and in vitro organ models: a review. Tissue Eng B: Rev 2013;19:529–543.
18. Miyoshi H, Ohshima N, Sato C. Three-dimensional culture of mouse bone marrow cells on stroma formed within a porous scaffold: influence of scaffold shape and cryopreservation of the stromal layer on expansion of haematopoietic progenitor cells. J Tissue Eng Regen Med 2013;7:32–38.
19. Wang H, Xie J, Lu C, Zhang D, Jiang J. Renal mucinous tubular and spindle cell carcinoma: report of four cases and literature review. Int J Clin Exp Pathol 2015;8: 3122–3126.
20. Kishimoto TE, Yashima S, Nakahira R, Onozawa E, Azakami D, Ujike M, Ochiai K, Ishiwata T, Takahashi K, Michishita M. Identification of tumor-initiating cells derived from two canine rhabdomyosarcoma cell lines. J Vet Med Sci 2017;79: 1155–1162.
21. Huang B, Bates M, Zhuang X. Super resolution fluorescence microscopy. Annu Rev Biochem 2009;78:993–1016.